ELSEVIER

Surface Science 359 (1996) 135–146

surface science

Bonding geometries of F and Cl on Si(100)-2 × 1

W.C. Simpson [a,b,1], J.A. Yarmoff [a,b,*]

[a] *Department of Physics, University of California, Riverside, CA 92521, USA*
[b] *Materials Science Division, Lawrence Berkeley National Laboratory, Berkeley, CA 94720, USA*

Received 17 July 1995; accepted for publication 12 January 1996

Abstract

Angle- and energy-resolved F^+ and Cl^+ electron-stimulated desorption distributions are collected from Si(100)-2 × 1 surfaces exposed at room temperature to XeF_2 or Cl_2. These distributions are fit to a model that accounts for ion–surface interactions in order to extract bond angle information. It is found that both F and Cl chemisorb on the dangling bonds of intact Si dimers, at an angle of ~20° from normal along the [011] azimuth. By annealing a chlorinated surface above ~400 K, some normally oriented Si–Cl bonds are generated. In addition to determining bonding geometries, quantitative information is obtained regarding the image–charge interaction and neutralization for F^+ and Cl^+ interacting with Si.

Keywords: Angle resolved DIET; Chemisorption; Halogens; Ion–solid interactions; Low index single crystal surfaces; Silicon

1. Introduction

Many surface science techniques, including electron- and photon-stimulated desorption (ESD/PSD), low-energy ion scattering (LEIS) and secondary ion mass spectrometry (SIMS), utilize low-energy ions to probe surfaces. Often, the ions used in these studies are perturbed by the surface via the image–charge potential and neutralization to the point that what is measured far from the surface does not directly reflect the ion distribution near the surface. The relative effects of these ion–surface interactions are enhanced as the ion's kinetic energy decreases and cannot be safely neglected for processes in which the energy of the ion is only a few eV, as is the case for stimulated desorption.

Recently, a new approach to the collection and interpretation of ESD ion angular distributions (ESDIAD) has been developed which offers a means of quantifying the interactions of low-energy ions with a surface [1]. In this approach, both energy-resolved angular distributions and angle-resolved kinetic energy distributions of ESD ions are collected and fit to a theoretically derived lineshape that explicitly includes the effects of the image–charge interaction and anisotropic neutralization. This differs from the traditional ESDIAD methodology [2,3], which typically involves collecting energy-integrated angular distributions or angle-integrated kinetic energy distributions, in that the increased spectral resolution enables a quantitative measurement of the effects of ion–surface interactions.

Once these effects are quantified, a more precise

* Corresponding author.
[1] Present address: Environmental Molecular Science Laboratory, Pacific Northwest, National Laboratory, Richland, WA 99352, USA.

PII S0039-6028(96)00373-1

determination of the initial angle of ion emission, and hence the orientation of the surface bonds, can be made. Because of its simple geometry (with primarily normal bonding), Cl_2/Si(111)-7 × 7 was investigated in Ref. [1] as a model system for testing the validity of this new approach. With the bond angle known a priori for that system, emphasis was placed on determining the strength of the initial image–charge interaction and the degree of anisotropy in the neutralization.

Now that reasonable values for these parameters are known, this approach is applied to two systems with more complex geometries – F/Si(100)-2 × 1 and Cl/Si(100)-2 × 1. F and Cl atoms both attach to the dangling bonds of the Si dimers that comprise the Si(100)-2 × 1 surface, preserving the 2 × 1 reconstruction [4]. The ESD ions emitted from these sites generate four off-normal ESDIAD emission lobes, reflecting the symmetry of the orthogonal domains of dimer sites [5–14].

The bonding geometry of Cl on Si(100) is, however, more complex than for F. The ESDIAD pattern of Si(100) chlorinated at low temperatures (~120 K) exhibits an additional normally oriented Cl^+ lobe, which indicates an additional bonding configuration, other than attachment to an intact Si dimer [8,9]. In addition, there is some evidence suggesting that normally oriented Si–Cl bonds are produced on Si(100) following chlorination at 500 K [15].

In the present study, it is found that adsorption of both F and Cl on Si(100) at room temperature results in Si–X bonds tilted ~20° from normal along the [011] azimuth (i.e., parallel to the dimer direction), consistent with bonding solely at the dangling bond sites of intact dimers. In addition to obtaining bonding geometries from the data, the effects of ion–surface interactions in the ESD of F^+ and Cl^+ from Si(100) are quantified, providing new insight into how these interactions shape the measured ion distributions.

2. Experimental procedure

The measurements were carried out in an ultra-high vacuum (UHV) chamber equipped with an electron gun, a hemispherical electrostatic energy analyzer (ESA), a quadrupole mass spectrometer (QMS), and a four-grid low-energy electron diffraction (LEED) system that is also used for Auger electron spectroscopy (AES) measurements. Single crystal Si(100) wafers (*n* type, ~1 Ω·cm, ±0.25°) were mounted on a manipulator that allows for sample rotation through an axis parallel to the surface, so that ions and electrons can be collected as a function of the polar angle relative to the surface normal. The samples were oriented such that all off-normal measurements were made along the same azimuth, within ~1° of [011], as determined with LEED. The Si samples were cleaned by resistive heating to ~1300 K. Sample cleanliness was checked by AES and LEED. Clean Si surfaces could be repeatably prepared which had no measurable oxygen or carbon contamination and which exhibited extremely sharp LEED patterns consisting of both (2 × 1) and (1 × 2) diffraction spots.

Samples were exposed in situ to atomic F via XeF_2 vapor [16], or to a collimated beam of Cl_2 produced by a solid-state AgCl electrochemical cell [17]. All exposures were carried out with the sample at room temperature. In all cases, the LEED patterns obtained from the halogenated surfaces maintained their original (2 × 1) symmetry, although the diffraction spots were often not as intense nor as sharp as those from the clean surfaces.

In order to determine Cl coverages, a Cl/Si AES ratio was obtained for each surface by collecting first-derivative AES spectra with a 3-keV incident electron beam and taking the ratio of the Cl(LMM) to Si(LMM) peak-to-peak intensities. This measured Cl/Si AES ratio is proportional to the Cl coverage as long as no multilayer growth occurs. To convert to Cl coverage, the Cl/Si AES ratio of 0.92 found for a Cl_2-saturated surface is assumed to correspond to the saturation coverage of $\Theta_{Cl} = 1.33$ monolayers (ML), which was determined via photoelectron spectroscopy [18].

In preparing the fluorinated surfaces, only very low exposures of XeF_2 were used, in order to minimize etching-induced disorder. The small amount of adsorbed F ($\leq$0.25 ML) makes it difficult to determine the coverage accurately. Also, due to the high cross-section for F removal via ESD, AES spectra cannot be collected from these surfaces. Instead, measured variations in the work

function, $\Delta\phi$, are correlated with F coverages, Θ_F, via the relation

$$\Delta\phi = (p_{SiF}\Theta_F)/(\epsilon_0\alpha), \quad (1)$$

where p_{SiF} is the dipole moment of a Si–F bond ($\sim 4\times10^{-30}$ C·m) and α is the area of the unreconstructed Si(100) surface unit cell (~ 15 Å^2) [19]. Any inaccuracies in the reported F or Cl coverages due to the methods of calibration are not important, however, since coverage is used here only as a convenient label.

The Cl^+ and F^+ ESDIAD measurements were made using the ESA, in constant-pass-energy mode, with a total energy resolution of better than 0.5 eV and an angular resolution of $\sim 4°$. To monitor changes in the work function, secondary electron cutoffs were collected by reversing the polarity of the appropriate elements in the ESA. The sample was biased +10 V relative to the analyzer when measuring ions and −10 V when measuring electrons so that the vacuum level (VL) of the analyzer was well below that of the sample. This way, the VL of the analyzer itself does not directly affect the shape of the measured kinetic energy distributions. Care was taken to position the sample relative to the ESA so that ions and electrons were collected directly above the electron beam spot on the sample. All measurements were carried out at room temperature.

The ion distributions were measured in two ways. First, energy-resolved angular distributions were collected by rotating the sample relative to the analyzer, with the ESA set to monitor a particular ion kinetic energy. For display purposes, the reported angular distributions are folded about the surface normal direction to reflect the two-fold symmetry of the surface along the [011] azimuth. Second, angle-resolved ion kinetic energy distributions (IKEDs) were collected by ramping the energy detected by the ESA while keeping the angle of detection fixed. Note that the work function difference between the sample and analyzer, which varies with adsorbate coverage, introduces an offset between the VLs of the sample and analyzer, so that the measured kinetic energy of an ion is not the energy it has near the surface. To account for this offset, secondary electron cutoffs collected from each surface were used to correct the energy scale (see Ref. [1]), so that all reported kinetic energies are given with respect to the surface VL.

Care was taken to minimize electron beam damage during the measurements. A 300-eV electron beam was used to excite both the ESD ions and the secondary electrons for the cutoff measurements. The total current on the sample was ~ 10 nA, in a spot size of ~ 1 mm diameter, with a typical collection time of 800 s. For collecting AES spectra, the current on the sample was ~ 1 μA, in a spot size of ~ 2 mm, with a typical collection time of 200 s. The AES measurements were always carried out after the ESD measurements because the higher energy and current of the AES beam is likely to cause the most beam damage.

Fluorine contamination is a major concern in ESD experiments utilizing Si substrates. In fact, even after heating well above the F desorption temperature, F can be found in sufficient quantities on a Si surface for F^+ ESD experiments to be carried out without intentionally exposing the surface to F [6,7]. Moreover, the high ESD cross-section enables the F^+ signal from a trace amount of F to easily match the intensity of ESD ions generated by larger quantities of another adsorbate. An example of this is shown in Fig. 1, which contains angle-resolved kinetic energy distributions of positive ions collected from a Si(100)-2 × 1 surface that was exposed at room temperature to Cl_2 to attain a Cl coverage of 0.05 ML, but which was not intentionally exposed to any F. Since F^+ and Cl^+ ions have distinct, well-separated kinetic energy distributions, the contribution to the positive ion signal from each of these species is easily identified [18]. It can be seen from the Fig. 1 that F^+ peaks in intensity $\sim 20°$ from normal, whereas the Cl^+ yield peaks near normal. Furthermore, at many angles of detection, the F^+ and Cl^+ yields are comparable.

In order to avoid any uncertainties introduced by the possibility of contamination, ESD ions were also measured with the QMS by turning its ionizer off and collecting the mass distribution of positive ions emitted at various polar angles along the [011] azimuth. In these measurements, only F^+ and Cl^+ ions were ever detected with the QMS, although the measurements were insensitive to H^+.

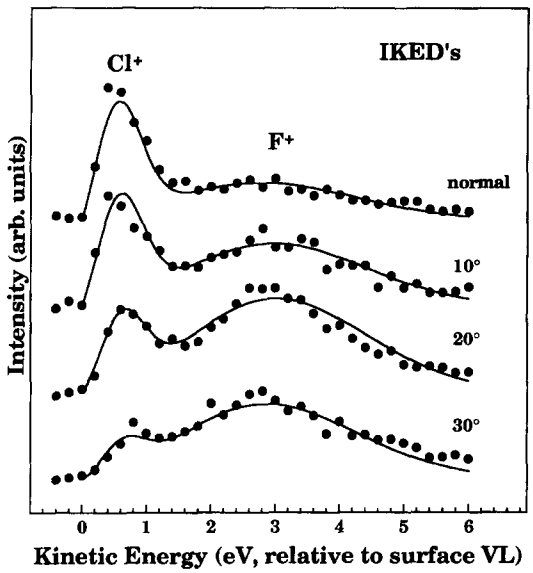

Fig. 1. Positive ion kinetic energy distributions from Si(100)-2 × 1 dosed with Cl_2 to a coverage of 0.05 ML, collected at four different polar angles along the [011] azimuth. The filled circles and triangles are the raw data and the solid lines show fits to the data.

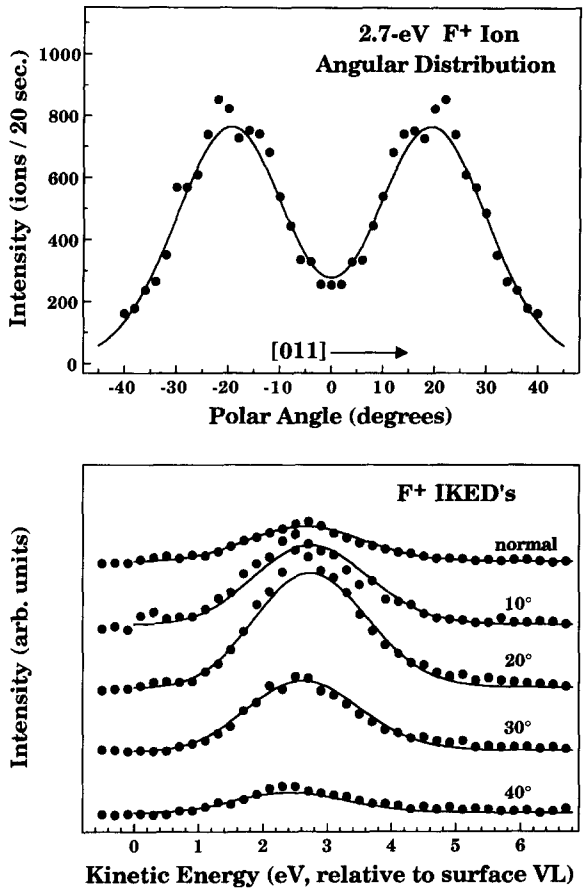

Fig. 2. (a) The angular distribution of 2.7-eV F^+ ions desorbing from a Si(100)-2 × 1 surface dosed with XeF_2 to a F coverage of ~0.2 ML, collected along the [011] azimuth. (b) F^+ kinetic energy distributions collected from the same surface at five different polar angles along the [011] azimuth. The filled circles are the raw data and the solid lines show fits to the data.

The F^+ ion intensity peaked at ~20° from normal, with a nearly undetectable contribution at normal emission. Cl^+, instead, had the highest signal normal to the surface, with little measurable intensity at angles greater than ~30°. The correlation of the QMS angular distributions with those collected using the ESA further support the identification of Ref. 18, i.e., that the ~1-eV ions are Cl^+ and the ~3-eV ions are F^+ (see Fig. 2).

Only contamination-free surfaces were used in this investigation. To rule out pre-existing contamination on the starting surfaces, especially H^+, which could not be identified directly with the QMS, positive ions were collected from samples prior to halogen exposure with both the ESA and the QMS. Clean surfaces were prepared by repeatedly annealing Si(100) wafers to 1300 K until no positive ion yield was detected with either the ESA or the QMS. Likewise, the IKEDs collected from the halogenated surfaces contained only single peaks whose shape and energy are consistent with either F^+- or Cl^+-stimulated desorption from Si [5–7,9,18], and they contained no additional features which could be attributed to H^+ or to any other contaminant.

A bias of 10 V was applied between the sample and the ESA during measurement, in order to obtain an ion yield with reasonable signal-to-noise as well as to correct for the difference in work function between the sample and detector. This bias voltage generally has two effects on the positive ion distributions. First, it increases their measured kinetic energy. Second, it generates an electric field between the sample and the analyzer which, to first order, increases the effective acceptance angle of the ESA by focusing the ions toward its

entrance aperture. A comparison of ion distributions collected from identical surfaces, using different values for the bias, showed that the distributions change somewhat with the bias voltage. It is likely that this is due to weak electric fields between the sample and metal elements in the UHV chamber which slightly alter the trajectories of the low-energy ions. This problem, which has been noted by other investigators [10], is endemic to the study of low-energy ions. Based on a comparison of data collected with different bias voltages, however, it is estimated that these stray fields introduce a systematic error of no more than 2–3° in the reported bond angles.

3. Experimental results

Fig. 2 shows energy and angular distributions of F^+ ions desorbing from Si(100)-2 × 1. Fig. 2a shows the angular distribution of 2.7-eV F^+ ions and Fig. 2b contains F^+ IKEDs collected from the same surface, at 10° intervals along the [011] azimuth. The data in Fig. 2 are representative of the F^+ distributions collected in this study, in that the mean measured F^+ kinetic energy is ~2.7 eV and the measured angular distribution is peaked ~20–25° from normal.

Fig. 3 contains energy and angular distributions of Cl^+ ions collected from a Si(100)-2 × 1 surface covered with 0.2 ML of Cl. The angular distribution of 0.7-eV Cl^+ ions is shown in top panel, and angle-resolved IKEDs are shown in the bottom panel. These data are typical of those collected from Si(100) following room-temperature Cl_2 adsorption. Note that the mean measured kinetic energy of Cl^+ desorbing from Si(100)-2 × 1 (~0.8 eV) is considerably lower than that of F^+, and that the measured angular distribution is typically very broad and exhibits maxima ~10° from normal. Further, note that, due to the lower angular resolution used in this study, the Cl^+ angular distributions appear much broader than those collected in earlier ESDIAD investigations of Cl/Si(100) [8–10,13,14], which makes it difficult to resolve the double-humped structure.

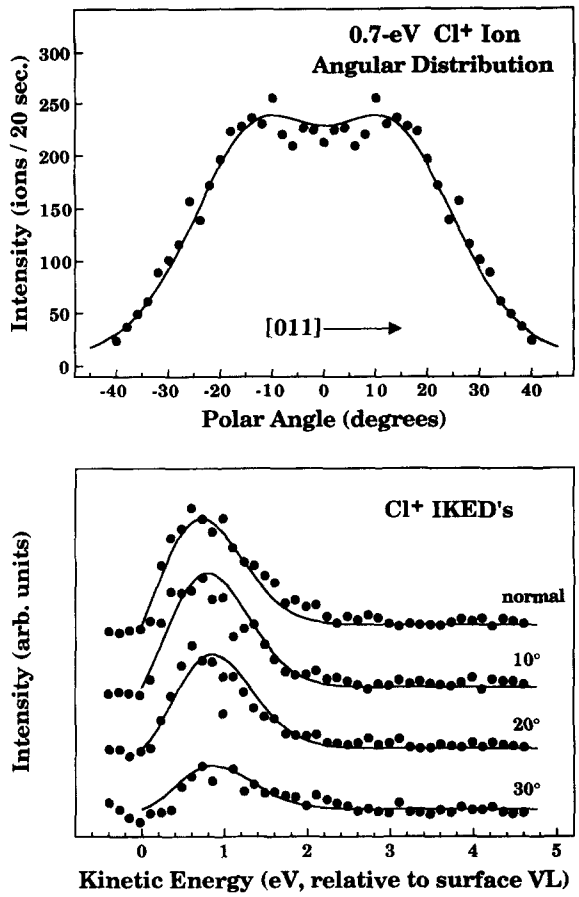

Fig. 3. (a) The angular distribution of 0.7-eV Cl^+ ions desorbing from a Si(100)-2 × 1 surface dosed with Cl_2 to a coverage of ~0.2 ML, collected along the [011] azimuth. (b) Cl^+ kinetic energy distributions collected from the same surface at four different polar angles along the [011] azimuth. The filled circles are the raw data and the solid lines show fits to the data.

4. Analysis

Data similar to those shown in Figs. 2 and 3 were collected from surfaces prepared with a range of F and Cl coverages and fit to a model that accounts for the distorting effects of ion–surface interactions. This model, which is described in detail in Ref. [1], specifically incorporates two effects: (1) the deflection and possible recapture of ions by the image-charge potential; and (2) anisotropic neutralization of the ions by the surface. The image–charge interaction is characterized by a single parameter, W, which is the strength of

the image–charge potential when the ion is first formed. Anisotropy in the neutralization of desorbing ions is accounted for with an angular-dependent ion survival probability factor, P^+, put forth by Hagstrum [20],

$$P^+ = \exp\left[-\left(\frac{V}{v_0}\right)\left(\frac{1}{\cos\theta_0}\right)\right], \quad (2)$$

where v_0 is the initial velocity of the ion, θ_0 is its initial desorption angle, and V parameterizes the degree of off-normal neutralization. The image–charge interaction deflects ions away from normal, whereas the anisotropic neutralization preferentially removes off-normally emitted ions [21,22]. The balance between these two effects ultimately determines the shape of the measured ion distributions.

The effects of the image–charge interaction and neutralization are combined to generate a theoretical lineshape, parameterized by W and V, which describes the angle- and energy-resolved ion distributions. Other parameters that serve to define the lineshape are the mean kinetic energy, mean desorption angle and the full-width at half-maximum (FWHM) of the initial ion kinetic energy and angular distributions. Bonding geometry information is obtained from the fit parameters by equating the mean initial desorption angle with the original bond angle on the surface prior to desorption, which is the fundamental assumption used in interpreting ESDIAD data.

The lineshape used to fit the F^+ and Cl^+ data is specific to a particular bonding geometry, i.e., one with two off-normally oriented Si–X bonds symmetrically arranged about the surface normal along the [011] azimuth. This is the simplest, physically realistic lineshape that yields adequate fits to all of the data. For reasons discussed below, normally emitted Cl^+ is not explicitly included in the lineshape, nor is the Cl^+ signal originating from the orthogonal domains of Si-Si dimers (i.e., those oriented along the $[0\bar{1}1]$ azimuth). Values for the mean initial ion kinetic energy, $\bar{E}_0$, the bond angle, $\bar{\theta}_0$, the initial image–charge interaction strength, W, and the neutralization parameter, V, were determined by fitting this lineshape simultaneously to the energy- and angle-resolved ESD data collected from each surface. The quality of the resulting fits is illustrated in Figs. 2 and 3, in which the fits to the data are shown as solid lines. Surprisingly, it is found that the parameters obtained from this procedure fluctuate only slightly around well-defined average values, with no trends readily apparent as the adsorbate coverage is changed. This is illustrated in Fig. 4, which shows the derived Si–Cl and Si–F bond angles plotted as a function of adsorbate coverage.

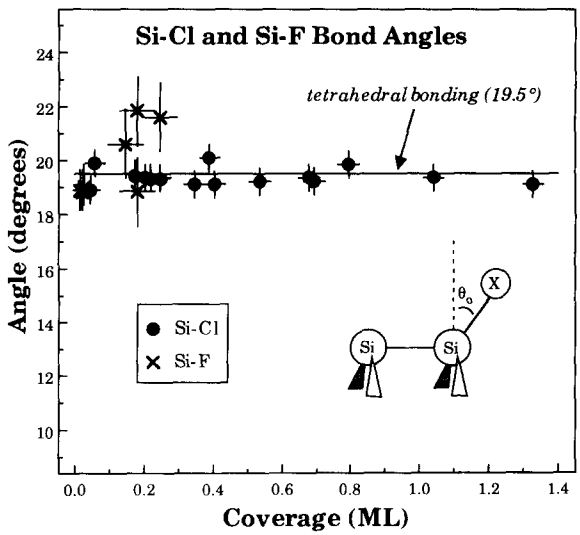

Fig. 4. Si–Cl and Si–F bond angles determined for the Si(100)-2 × 1 surface at various F and Cl coverages. Filled circles and crosses are the Si–Cl and Si–F bond angles, respectively. The solid line indicates the angle for ideal tetrahedral bonding.

The average values of the principal fit parameters are given in Table 1, for F^+ and Cl^+ desorption from Si(100)-2 × 1 and for Cl^+ desorption from Si(111)-7 × 7 (from Ref. 1). The error bars represent statistical fluctuations about the mean value and do not include any consideration of systematic errors, such as those introduced by the choice of lineshape or by the bias voltage applied between the sample and detector. Several things are readily apparent from Table 1. Most important to note is that F^+ and Cl^+ desorbing from Si(100) have similar initial desorption angles ($\sim 20°$), indicating that F and Cl have nearly identical bonding geometries on this surface. The bonding configurations most consistent with a Si–X bond tilted $\sim 20°$ from

Table 1
Average values of the bond angle, angular FWHM, mean initial kinetic energy ($\bar{E}_0$), energy FWHM, initial image–charge interaction strength (W), and neutralization parameter (V) for F^+ and Cl^+ ions desorbing from a Si(100) surface, as determined from fits to the data

Ion	Substrate	Bond angle	Angle FWHM	$\bar{E}_0$ (eV)	Energy FWHM (eV)	W(eV)	V(10^5 m/s)	θ_c ($\bar{E}_0$)
F^+	Si(100)-2×1	20.0±1.3°	22–27°	7.2±0.4	2.4–2.8	4.4±0.4	1.6±0.1	39°
Cl^+	Si(100)-2×1	19.3±0.3°	20–25°	4.4±0.1	1.5–2.0	4.0±0.2	12.0±0.5	18°
Cl^+	Si(111)-7×7	0°	25°	4.6	1.2	3.6	10.4	28°

The parameters for the Si(111) surface are from Ref. [1]. Also reported are the critical angles for desorption at the mean initial kinetic energy, for each of the systems studied. Error bars indicate the statistical fluctuations about the mean value, and do not include systematic errors.

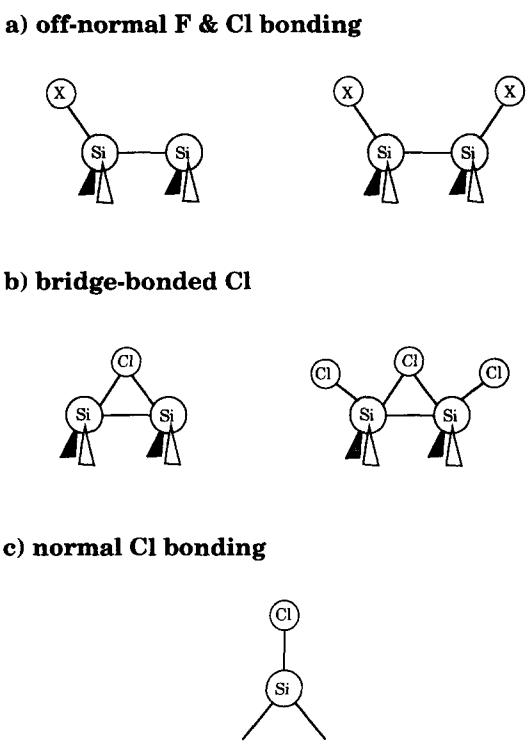

Fig. 5. Illustrations of the possible bonding configurations of Cl on Si(100). (a) The two types of off-normal bonding expected for the 2×1 surface. (b) Two types of bridge-bonded Cl expected at low temperatures. (c) A normally oriented Si–Cl bond in an sp^2-like configuration.

normal are shown in Fig. 5a. In both cases, the halogen is attached at a dangling bond site of an unbroken Si dimer.

In Table 1, it is seen that the image–charge interaction strengths follow expected behavior. That is, since ionization occurs at the adsorption site, atoms bonded closest to the surface should have the largest initial image–charge interaction. Cl atoms bonded normally on Si(111) are located farther from the surface than Cl atoms bonded off-normally on Si(100) which, in turn, are farther from the surface than F atoms on the (100) surface, given that the Si–F and Si–Cl bonds are tilted at roughly the same angle and that Si–F bonds are generally shorter than Si–Cl bonds [19]. Consequently, the initial image–charge interaction strength should be the greatest for F^+ desorbing from the (100) surface and the least for Cl^+ desorbing from the (111) surface, consistent with the results shown in Table 1.

From the values of V in Table 1, it is seen that the anisotropy in the neutralization of Cl^+ ions is similar for Si(111) and (100). There is, however, nearly an order-of-magnitude difference in the values of V found for Cl^+ and F^+ on Si(100). The parameter V is sensitive to how the neutralization rate drops off with distance above the surface [1]. The much larger value of V for Cl^+ may indicate that there is an additional neutralization mechanism for Cl^+ (e.g., resonant neutralization), or it may be a size effect related to the larger ionic radius of Cl^+.

Also listed in Table 1 is the critical angle for desorption at the mean kinetic energy, $\theta_c(\bar{E}_0)$. The critical angle for desorption is defined such that ions with energy E_0 desorbing at angles greater than $\theta_c(E_0)$ have insufficient momentum perpendicular to the surface to overcome the attractive image–charge interaction and are thus recaptured, whereas ions desorbing at angles less than θ_c are able to escape the surface (see Refs. [1,21]). The

critical angle is a function of the ion's initial energy,

$$\theta_c = \cos^{-1}\left(\sqrt{\frac{E_0}{W}}\right), \quad (3)$$

and since there is a spread in initial ion kinetic energies (FWHM ~ 25°), there is a corresponding spread in critical angles, roughly centered about $\theta_c(\bar{E}_0)$. For F^+, with a Si–F bond angle of 20°, a critical angle for desorption of 39° indicates that very few F^+ ions are recaptured by the surface. Cl^+ desorbing from the (100) surface has an initial angular distribution similar that of F^+. However, Cl^+ has a much lower mean initial kinetic energy than F^+, leading to a smaller critical angle for desorption. In fact, for the (100) surface, the critical angle for Cl^+ desorption is only 18°, which is less than the derived Si–Cl bond angle of 19.3°, indicating that Cl^+ ions desorbing with the mean initial kinetic energy along the original bond direction do not escape the surface. This being the case, without the finite widths of the initial Cl^+ energy and angular distributions, no Cl^+ would be detected at all, and the magnitude of these widths predominantly determines the shape of the measured distributions. This, combined with the order-of-magnitude difference in their neutralization parameters, illustrates why Cl^+ angular distributions have little off-normal emission compared to F^+ distributions from Si(100), as well as why the Cl^+ ESD yield from Si is generally much less than that of F^+. It also rules out any Cl^+ signal being detected from adsorbed $SiCl_2$ (with Si–Cl bond angles of ~55° from normal), or from any other species having Si–Cl bonds tilted more than about 25° from normal [1].

5. Discussion

Because F etches Si at room temperature, investigations of F^+ desorption were limited to the low-coverage regime in which there is the least amount of etching-induced damage. In fact, even though care was taken to minimize etching, it is possible that some did occur on the Si samples with F coverages above ~0.1 ML. Judging from the scatter in the Si–F bond angle for surfaces with similar F coverages (Fig. 4), and noting the larger spreads in energy and angle for F^+ than for Cl^+ (Table 1), it is likely that the fluorinated surfaces have suffered some disordering.

The Si–F bond angle of 20°, derived in this study from measured emission angles of 20–25°, is somewhat lower than values obtained in previous investigations. Two prior F^+ ESDIAD studies of F/Si(100)-2 × 1 [6,7] and one of HF/Si(100)-2 × 1 [11], report field-free F^+ emission angles ranging from 29 ± 3 to 36 ± 5°. In those studies the field-free emission angle was equated with the Si–F bond angle. It is interesting to note that in the present investigation, which carefully accounts for the effects of ion–surface interactions, the derived Si–F bond angle is found to be very close to the field-free F^+ emission angle. Thus, in the case of F/Si(100), the distorting effects of anisotropic neutralization and the image-charge interaction fortuitously balance out, yielding a measured angular distribution that is similar to the initial one.

The analysis of the Cl^+ data is more complicated than for F^+. In contrast to F^+, the Cl^+ distributions are strongly affected by ion–surface interactions. Moreover, the Cl^+ distributions may have additional contributions from Cl^+ emitted along the surface normal, as this has been observed under certain conditions [5,6,8–10,13,14]. In order to determine whether such contributions are present after room-temperature Cl_2 adsorption, two tests were carried out in which chlorinated surfaces were either bombarded with electrons or annealed. The effects of these treatments on the ESDIAD behavior are then compared to the findings of similar experiments in order to identify the origin of normally emitted Cl^+ and, ultimately, to rule out the possibility of normally emitted Cl^+ contributing significantly to the present data.

A normal emission Cl^+ ESDIAD lobe has been observed previously under two extreme conditions. In the first, surfaces were prepared and examined at low temperatures, typically at ~120 K [8–10,13,14]. In the second, chlorinated surfaces were annealed above room temperature [5,6,9,10,13]. Normal emission is thought to result from a unique bonding configuration in each case, as discussed below.

There is clear evidence supporting the notion

that the low-temperature normal emission is due to bridge-bonded Cl atoms, in configurations such as those illustrated in Fig. 5b [8,9,23,24]. Since bridge sites are energetically less stable than the dangling bond sites of the dimer atoms [24], surfaces containing bridge-bonded Cl must be prepared at low temperature. The instability of the bridging configuration makes it an unlikely site for room-temperature adsorption. If, however, a limited number of these sites were indeed generated on Si(100) by room-temperature chlorination, they might still contribute measurably to the Cl^+ signal, given their high ESD cross-section relative to off-normally bonded Cl [9]. To test this hypothesis, a Si(100) wafer was dosed with Cl_2 at room temperature to a coverage of 0.40 ML, and subsequently exposed to a defocused 3-keV electron beam in order to electronically desorb Cl from the surface. Evidence for a significant number of bridge sites being populated would appear as a noticeable change in the shape of the Cl^+ distribution, arising from the preferential removal of bridge-bonded Cl, as was observed by Gao et al. [9]. The results of this test are shown in Fig. 6. Bombardment of the surface with $\sim 4 \times 10^{17}$ e/cm^2 removed half of the adsorbed Cl (as determined with AES) without substantially changing the shape of the ion distribution. Hence, for surfaces prepared at room temperature there appears to be little contribution to the Cl^+ yield from bridge-bonded Cl.

A normal emission Cl^+ ESDIAD lobe has also been observed for chlorinated Si(100) heated above room temperature [5,6,9,10,13], and for samples continuously exposed to Cl_2 at elevated temperatures [25]. Since bridge-bonded Cl is higher in energy than Cl bonded to a Si dimer atom [24], it is difficult to reconcile how the bridge site could become preferentially populated through elevation of the surface temperature. Instead, it is likely that a different bonding configuration is responsible for normal Cl^+ emission from annealed surfaces.

To determine whether this other type of Cl bonding site contributes significantly to the room-temperature Cl^+ yield, angular distributions were collected from Si(100) saturated with Cl_2 at room temperature and from the same surface after annealing to 400, 500, and 600 K. These distributions are shown in Fig. 7, along with the net change in

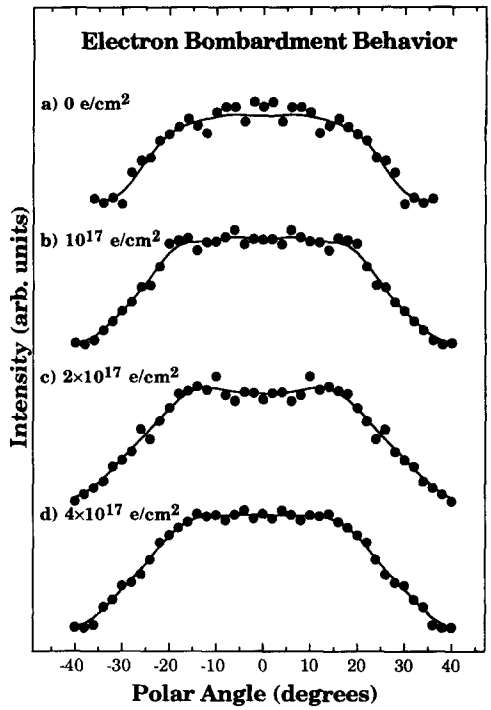

Fig. 6. Cl^+ angular distributions collected (a) from Si(100) covered with 0.40 ML of Cl, and from the same surface following exposure to (b) 10^{17} e/cm^2, which reduced the Cl coverage to 0.25 ML, (c) 2×10^{17} e/cm^2, which reduced the Cl coverage to 0.22 ML, and (d) 4×10^{17} e/cm^2, which reduced the Cl coverage to 0.20 ML.

the angular distribution due to annealing at 600 K. A noticeable contribution from normally emitted Cl^+ does appear after annealing to 500 K and above, indicating that a conversion from off-normal to normal Cl^+ emission occurs somewhere between 400 and 500 K.

This transition from off-normal to normal Cl^+ emission observed in ESDIAD correlates with the results of X-ray absorption experiments on Cl/Si(100). In those studies it was found that Si(100) surfaces chlorinated at room temperature have Si–Cl bonds tilted 20–25° from normal [15,26,27], whereas Si–Cl bonds on Si(100) chlorinated at 500 K lie within 10° of the surface normal direction, consistent with an atop geometry [15]. Hence, a conversion between the two types of bonding occurs at some intermediate temperature. It is therefore suggested that this transition from off-normal to normal Cl bonding is the cause for

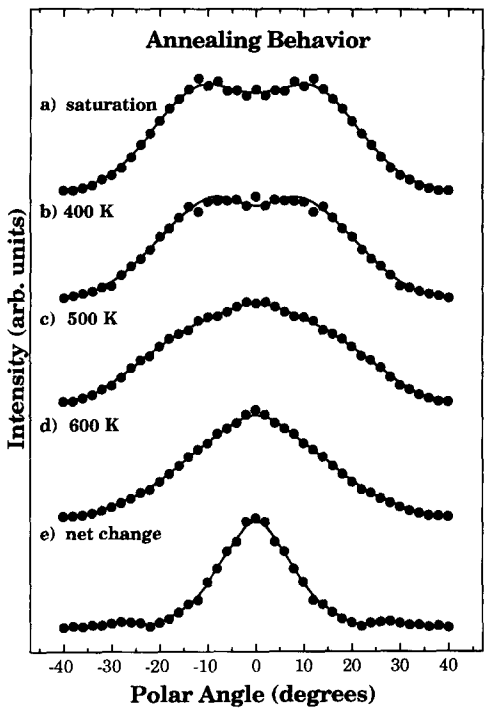

Fig. 7. Cl^+ angular distributions collected from a Cl_2-saturated surface, and from the same surface following annealing to 400, 500 and 600 K. Panel (e), which illustrates the net change in the angular distribution due to annealing to 600 K, was obtained by subtracting the distribution in panel (a) from that in panel (d), after scaling them to have equal intensity at 35°.

the observed conversion from off-normal to normal Cl^+ emission.

The exact mechanism for forming normally oriented Si–Cl bonds via annealing is unclear, as an ideal Si(100)-2 × 1 surface does not have any bonds directed along the surface normal. Since normal Si–Cl bonds are formed at elevated temperatures, it is likely that they result from etching, as suggested in Refs. [10,25]. A means of producing such bonds via etching is proposed which is consistent with the X-ray absorption and ESDIAD data. Since $SiCl_2$ is the primary thermal desorption product of chlorinated Si [28], heating chlorinated Si(100) must lead to the removal of surface Si atoms. If one atom in a dimer pair were removed in this fashion, the other would be left without a neighboring Si atom to which it can dimerize. Cl attached to such a lone Si atom would then cause it to rehybridize to an sp^2-like configuration, with the Cl bonded atop, as illustrated in Fig. 5c. Even if this were an unlikely process, so that relatively few of these sites were generated, they could still contribute measurably to the Cl^+ yield since the ESD cross-section for such a site is expected to be quite high, as in the case of the bridge-bonded Cl [9]. In addition to possible electronic enhancements, a larger cross-section is expected for normally emitted Cl^+ for two other reasons: (1) neutralization is greatly reduced normal to the surface, and (2) the angle of ion emission is well below the critical angle for desorption, so that none of the ions are recaptured.

Hence, the bonding configurations responsible for normally emitted Cl^+ have been identified and determined not to be present in measurable amounts following room-temperature Cl_2 adsorption. Consequently, the Cl^+ ESD lineshape used in this study only explicitly includes Cl^+ emission originating from off-normally oriented Si–Cl bonds. The quality of the fits and the consistency of the parameters derived from the fits further support the claim that this lineshape adequately describes the data (see Fig. 4 and Table 1).

As seen in Fig. 3, however, some Cl^+ signal is observed normal to the surface. This Cl^+ signal originates from off-normally oriented Si–Cl bonds that tilt toward the surface normal as a result of thermal vibrations. Half of the normal emission signal originates from Si–Cl bonds oriented along the [011] azimuth, while the other half arises from Si–Cl bonds directed along the $[0\bar{1}1]$ azimuth. As stated above, the signal originating from bonds oriented along the $[0\bar{1}1]$ azimuth is not explicitly included in the ESD lineshape, which introduces systematic errors in the numbers obtained from fitting the data.

An attempt was made to estimate the magnitude of these errors. An accurate determination of the contribution arising from Si–Cl bonds oriented along the $[0\bar{1}1]$ azimuth requires collecting ion distributions along more than one azimuth in order to obtain a measure of the azimuthal spread of the distributions. Unfortunately, since the azimuthal orientation of the sample is fixed on the manipulator used in this study, such measurements were not possible. Instead, the contribution to the angular distributions arising from Si–Cl bonds oriented

along the [0$\bar{1}$1] azimuth was assumed to be Gaussian in shape, centered about the surface normal, with its maximum equal to half of the intensity at the surface normal. Gaussian distributions with FWHMs ranging from 10 to 30° were subtracted from the raw Cl^+ angular distributions, and the distributions were then refit. It was found that the primary result of removing the signal originating from Si–Cl bonds oriented along the [0$\bar{1}$1] azimuth is a decrease of 2–3° in the FWHM of the initial angular distribution, $\Delta\theta_o$, and a slight (<10%) increase in the neutralization anisotropy parameter, V. In all cases, the bond angle was found to change by less than 1°. Future experiments are planned in which this source of systematic error will be eliminated by using a manipulator with both polar and azimuthal rotation capabilities to collect ion distributions along more than one azimuth. However, for the time being, it appears that ignoring the Cl^+ signal arising from the chlorinated [0$\bar{1}$1] dimers introduces only a small error in the fitting parameters.

The Si–Cl bond angle determined in this study compares well with values obtained in previous ESDIAD investigations of Cl_2/Si(100)-2×1, especially considering the differences in the apparatus, sample preparation and analysis techniques that were used. From a Cl^+ field-free emission angle of ~28°, Yates et al. derived a Si–Cl bond angle of 25±4° [8,9,14]. In one study, Williams et al. measured a field-free Cl^+ emission angle of 40±10°, which they attributed to a Si–Cl bond tilted more than 20° from normal [6]. In a more recent investigation, however, they report Cl^+ angular distributions peaking 20–30° from normal, leading to a bond angle of 25±5° [10]. The angle of ~19° found in the present study (based on a field-free emission angle of ~10°) is somewhat less than the previously determined values, but it is still within the error limits of the previous measurements.

An angle of ~20° from normal along the [011] azimuth, for both Si–F and Si–Cl bonds on Si(100)-2×1, is close to that expected for the geometries shown in Fig. 5a. Since halogens are expected to form directional monovalent bonds on Si, and since Si prefers a tetrahedral bonding geometry, the Si–X bond angle for intact dimers should be close to the ideal tetrahedral bonding angle of 19.5°. For illustration, a line has been drawn through the data in Fig. 4 to indicate this angle. Note that a recent theoretical investigation coincidentally predicts a Si–Cl bond angle of 19.3° from normal [24], although an earlier study calculated a somewhat smaller value (~15°) [29].

6. Conclusions

In this investigation, energy- and angle-resolved F^+ and Cl^+ electron-stimulated desorption distributions were collected from Si(100)-2×1 surfaces exposed at room temperature to XeF_2 or Cl_2. Using a new approach to interpret the ESD data, these distributions were fit to a model that accounts for ion–surface interactions in order to determine bonding geometries. Bond angles of 20.0 and 19.3° from normal along the [011] azimuth are derived for Si–F and Si–Cl, respectively, with a combined statistical-plus-systematic error of less than ±5°. Annealing a chlorinated surface above 400 K leads to the formation of some normally oriented Si–Cl bonds, likely as a result of etching. This approach also provides quantitative information about the image–charge interaction and neutralization, which is otherwise unavailable.

Acknowledgement

This work was supported by the Director, Office of Energy Research, Office of Basic Energy Sciences, Materials Science Division of the US Department of Energy under Contract No. DE-AC03-76SF00098.

References

[1] W.C. Simpson and J.A. Yarmoff, Phys. Rev. B 52 (1995) 2038.
[2] T.E. Madey, Science 234 (1986) 316.
[3] J.T. Yates, Jr., M.D. Alvey, M.J. Dresser, M.A. Henderson, M. Kiskinova, R.D. Ramsier and A. Szabó, Science 255 (1992) 1397.
[4] See D. Purdie et al., Phys. Rev. B 48 (1993), 2275; G.S.

Khoo and C.K. Ong, Phys. Rev. B 52 (1995) 2564, for a review of earlier structural studies.
[5] S.L. Bennett, C.L. Greenwood and E.M. Williams, in: Desorption Induced by Electronic Transitions, DIET V (Springer, New Mexico, 1993) p. 259.
[6] S.L. Bennett, C.L. Greenwood and E.M. Williams, Surf. Sci. 290 (1993) 267.
[7] M.J. Bozack, M.J. Dresser, W.J. Choyke, P.A. Taylor and J.T. Yates, Jr., Surf. Sci. 184 (1987) L332.
[8] C.C. Cheng, Q. Gao, W.J. Choyke and J.T. Yates, Jr., Phys. Rev. B 46 (1992) 12810.
[9] Q. Gao, C.C. Cheng, P.J. Chen, W.J. Choyke and J.T. Yates, Jr., J. Chem. Phys. 98 (1993) 8308.
[10] Q. Guo, D. Sterratt and E.M. Williams, Surf. Sci. submitted.
[11] A.L. Johnson, M.M. Walczak and T.E. Madey, Langmuir 4 (1988) 277.
[12] D. Sterratt, Q. Guo and E.M. Williams, Nucl. Instrum. Methods B 101 (1995) 84.
[13] D. Sterratt, Q. Guo and E.M. Williams, Surf. Rev. Lett. 1 (1994) 539.
[14] J.T. Yates Jr., C.C. Cheng, Q. Gao and W.J. Choyke, Surf. Sci. Rep. 19 (1993) 79.
[15] D. Purdie, N.S. Prakash, K.G. Purcell, P.L. Wincott and G. Thornton, Phys. Rev. B 48 (1993) 2275.
[16] H.F. Winters and F.A. Houle, J. Appl. Phys. 54 (1983) 1218.
[17] N.D. Spencer, P.J. Goddard, P.W. Davies, M. Kitson and R.M. Lambert, J. Vac. Sci. Technol. A 1 (1983) 1554.
[18] T.D. Durbin, W.C. Simpson, V. Chakarian, D.K. Shuh, P.R. Varekamp, C.W. Lo and J.A. Yarmoff, Surf. Sci. 316 (1994) 257.
[19] R.C. Weast, Handbook of Chemistry and Physics (CRC, Cleveland, OH, 1972).
[20] H.D. Hagstrum, Phys. Rev. 96 (1954) 336.
[21] Z. Miskovic, J. Vukanic and T.E. Madey, Surf. Sci. 141 (1984) 285.
[22] Z. Miskovic, J. Vukanic and T.E. Madey, Surf. Sci. 169 (1986) 405.
[23] J.J. Boland, Science 262 (1993) 1703.
[24] G.S. Khoo and C.K. Ong, Phys. Rev. B 52 (1995) 2574.
[25] Z. Dohnalek, Q. Gao, W.J. Choyke and J.T. Yates, Jr., Surf. Sci. 320 (1994) 238.
[26] G. Thornton, P.L. Wincott, R. McGrath, I.T. McGovern, F.M. Quinn, D. Norman and D.D. Vvedensky, Physica B 158 (1989) 640.
[27] G. Thornton, P.L. Wincott, R. McGrath, I.T. McGovern, F.M. Quinn, D. Norman and D.D. Vvedensky, Surf. Sci. 211/212 (1989) 959.
[28] A. Szabó, P.D. Farrall and T. Engel, Surf. Sci. 312 (1994) 284.
[29] P. Kruger and J. Pollmann, Phys. Rev. B 47 (1993) 1898.